Journal of Energy Storage 113 (2025) 115697

Contents lists available at ScienceDirect

Journal of Energy Storage

journal homepage: www.elsevier.com/locate/est

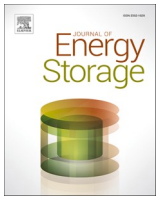

Research Papers

Model predictive control of large chiller plants for enhanced energy efficiency utilizing inherent cold storage of cooling systems

Xiaoyu Lin [a], Kui Shan [a,b], Shengwei Wang [a,b,*]

[a] Department of Building Environment and Energy Engineering, The Hong Kong Polytechnic University, Kowloon, Hong Kong
[b] Research Institute for Smart Energy, The Hong Kong Polytechnic University, Kowloon, Hong Kong

ARTICLE INFO

Keywords:
Chiller plant
Optimal control
Thermal storage
Model-based control
Deep-learning
Energy efficiency

ABSTRACT

In many practical situations, chiller plants often operate continuously. However, during low-demand periods, such as night hours and the end of working hours, they often run inefficiently, leading to significant energy waste. This issue is especially challenging for constant-speed chillers. In fact, utilizing the inherent cold storage to "force" the chillers to operate at high loads and high efficiency is a practically attractive option. Two innovative chiller control strategies are proposed for night hours and the end of working hours, respectively, leveraging the inherent cold storage in chilled water distribution networks. These strategies employ a model-based approach using deep learning to enhance the chiller energy efficiency while maintaining acceptable start-stop frequency. Their effectiveness is limited to scenarios with low cooling loads and appropriate distribution networks. The strategies are implemented and tested in a real central cooling system of a large commercial building. Field test results show that the proposed control strategies can reduce total chiller power consumption by 28.1 % during the night hours and by 14 % at the end of working hours.

1. Introduction

Chillers account for approximately 40 % of the total energy consumption in central air-conditioning systems [1]. Therefore, improving chiller efficiency is crucial for reducing energy consumption. In many practical scenarios, both existing and new chiller systems still use constant-speed chillers that are required to operate 24 h a day. During some periods, chillers must operate at low partial load ratios (PLRs). For example, this occurs during night hours when cooling demand remains low for extended periods, or during the end of working hours when cooling demand drops sharply, such as at the end of office hours (ending hours). This is a common issue in practical operations [2–5]. and the efficiency of constant-speed chillers is significantly impacted by low part-load ratios (PLRs) [6], leading to substantial energy waste.

To address this issue, several approaches have been proposed. One conventional solution involves using chillers equipped with variable speed drives (VSDs). The chiller speed is automatically adjusted to match the dynamic building cooling load, resulting in maintained high efficiency. However, VSDs consume approximately 4 % to 8 % of the energy they convert [7]. In addition, VSD chillers, especially high-voltage chillers (e.g., 11,000 V), require substantial upfront and maintenance costs [8].

Another effective approach is to utilize thermal energy storage (TES) systems. The TES system provides a practical solution by allowing the storage of excess cooling capacity during off-peak hours to reduce the peak cooling load of the chiller plant [9], when electricity rates and cooling demand are low [10–13]. A significant reduction of 38 % in electricity consumption was achieved by adjusting the operation hours of the TES system, cooling towers, pumps, and chillers to eliminate low-efficiency periods [14]. A small-scale TES system was integrated into a chilled water plant. Substantial energy savings were achieved with a model-based optimization control strategy across different weather conditions [15]. Another study used chilled water storage to improve the efficiency of large chiller plants with constant-speed-driven (CSD) chillers. The chiller efficiency was increased by 3.10 % and 22.94 % in summer and winter, respectively [8].

In addition to TES systems, various optimal control strategies have been proposed to improve the efficiency of central chiller plants. For example, an optimal strategy adopting simplified linear self-tuning models and genetic algorithms was proposed. Compared to a reference strategy that utilizes conventional settings, the optimal strategy resulted in daily energy savings of approximately 0.73–2.55 % for the studied system [16]. Another strategy was designed to optimize settings and

* Corresponding author at: Department of Building Environment and Energy Engineering, The Hong Kong Polytechnic University, Kowloon, Hong Kong.
E-mail address: beswwang@polyu.edu.hk (S. Wang).

https://doi.org/10.1016/j.est.2025.115697
Received 22 November 2024; Received in revised form 17 January 2025; Accepted 3 February 2025
Available online 8 February 2025
2352-152X/© 2025 The Authors. Published by Elsevier Ltd. This is an open access article under the CC BY-NC license (http://creativecommons.org/licenses/by-nc/4.0/).

Nomenclatures

Abbreviations

AHU	air handing unit
ARFIMA	autoregressive fractionally integrated moving average.
BMS	building management system
BPNN	back propagation neural network
CSD	constant-speed-driven
CV-RMSE	coefficient of variation of the root mean square error
FMI	functional mock-up interface
FMU	functional mock-up unit
LSTM	long short-term memory
MAE	mean absolute error
TES	thermal energy storage
PLR	part load ratios
POC	proof of concept
RNN	Recurrent Neural Network
VSD	variable-speed-driven

English symbols

C_{TES}	thermal capacitance of chilled water delivery system [kW]
$CL_{real-time}$	real time cooling load [kW]
CL_{1h}	cooling load for the next hour [kW]
$Mw_{,ev}$	evaporator water mass flow rate [L/s]
$Mw_{,cd}$	condenser water mass flow rate [L/s]
ΔT	allowed temperature increase of the chilled water [°C]
t_{off}	discharging time needs to be predicted [h]
T_{rtn}	return chilled water temperature [°C]
T_{sup}	supply chilled water temperature [°C]
$T_{sup,sp}$	supply chilled water temperature set-point [°C]
$y(k)$	actual value
$y_p(k)$	predicted value
$\bar{y}$	average value

minimize energy consumption in the chilled water pump for a chilled water system incorporating intermediate heat exchangers. Results demonstrated energy savings ranging from 5.26 % to 14.69 % compared to conventional strategies [17]. Another study evaluated the impact of chiller design and control strategies on the energy efficiency of a chiller plant with multiple chillers. Chiller performance curves were utilized as control inputs to determine each chiller's operation. The results indicated that the hourly sequencing control performed better than the weekly sequencing control [18].

Existing studies on TES systems mainly focus on independent energy storage systems. There are few studies on the energy-saving potential of chilled water distribution networks, this may be due to the limited cooling storage capacity of the water in the distribution pipes [19]. Yan et al. investigated retrofitting fire service water tanks as chilled water storage to reduce power demand and costs. These retrofit schemes offer easy implementation in existing buildings, resulting in substantial peak demand cost reductions and a payback period of three years [20]. However, the thermal storage capacity of chilled water distribution networks in centralized cooling systems has not been thoroughly explore, specifically concerning improving the energy efficiency of chillers.

Therefore, this study aims to optimize chiller operation by utilizing the thermal storage capabilities of distribution networks during low part-load ratio conditions. Two control strategies are proposed for night and end-of-working hours, integrating a physical logic-based control approach with a data-driven predictive model. These strategies enhance the efficiency of chillers by temporarily shifting the load to the distribution network. Meanwhile, they regulate the chillers to operate at high partial load rates, thereby boosting the overall system efficiency. While this study investigated the chiller plant efficiency under the proposed control strategy, the long-term reliability of chiller performance under serval times of start and stop in the night hours mode is not analyzed in this work. The major contributions of this study include:

- Demonstrating the feasibility of utilizing the thermal energy storage capacity of the chilled water distribution network to enhance chiller efficiency, particularly during night hours and end-of-working hours;
- Proposing two optimal control modes for different working conditions, enhancing chiller efficiency while maintaining indoor thermal comfort;
- Developing a predictive deep learning method to ensure that the thermal storage system carries the cooling load without the use of a chiller plant and avoids frequent chiller switching;
- Validating the proposed control strategy on-site in a real high-rise commercial building and on a simulation platform.

2. Model predictive control strategies and load prediction model

2.1. Basic idea and mechanism of energy saving utilizing system inherent cold storage

Chiller efficiency is highly related to the operating part load ratio (PLR) [21]. The COP of the CSD chiller, based on actual operating data, increases with increasing PLR. The proposed control strategy utilizes the thermal energy storage effect of the chilled water delivery system to improve the chiller efficiency. The fundamental idea of the proposed strategy is to maintain a high PLR of operating chillers based on real-time measurements and predicted working conditions. The control strategy also needs to keep the supply chilled water temperature within the allowed range so that the building thermal comfort is not compromised. To achieve a high PLR, the key approach is to delay the start of idle chillers, put forward the stop of running chillers, and optimize the set-point for the supply chilled water temperature [22]. Energy saving can be achieved in two ways: increased overall chiller efficiency and less operation time of the associated cooling water pumps and primary chilled water pumps.

Leveraging the inherent cold storage capacity of the cooling system to enhance chiller efficiency essentially involves load shifting. The fundamental mechanism operates in two steps.

1) *Charging*: To store cooling energy in the distribution network, the supply chilled water temperature is reduced when the chiller runs at a lower PLR, and temperature of the chilled water in the distribution network is lowered. This enhances the system's efficiency and capacity to meet cooling demands during off-peak periods.
2) *Discharging:* As the chilled water temperature of the distribution network rises, the efficiency of the chiller plant is gradually reduced. The discharging step begins by shutting down the chiller and the primary pump while sustaining the operation of the secondary pump. During the discharging step, the cooling energy stored in the distribution network is released to meet the cooling load on the demand side, which increases the chilled water temperature.

Fig. 1 illustrates the charging and discharging process of the inherent thermal storage. As the discharging process unfolds, when the chiller plant and primary pumps are shut off, the flow of chilled water is redirected in the bypass, and the temperature of the network gradually increases. This signifies the transfer of cooling energy from the pipework to the demand side. The charging process enhances the chiller's efficiency, while the discharging process reduces the chiller's operating duration.

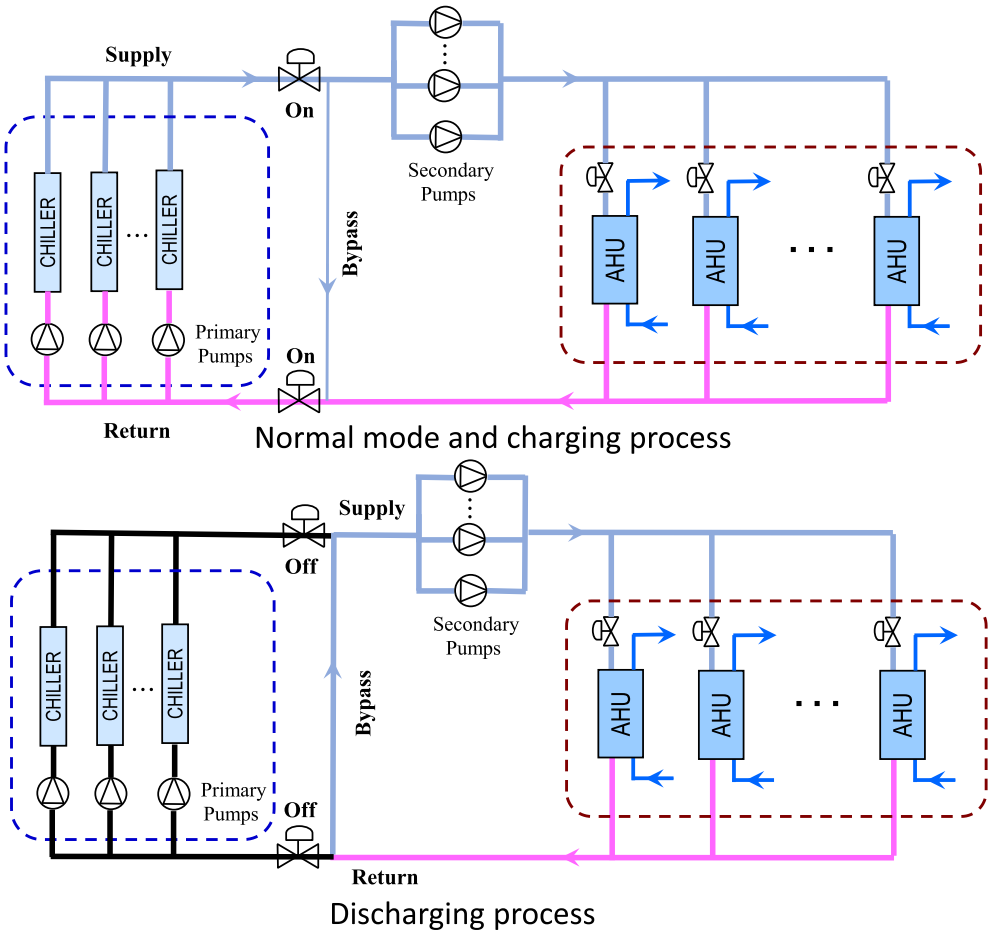

Fig. 1. The charging and discharging process of inherent thermal storage.

The inherent cold storage capability of the system can be utilized in two scenarios: night hours (low cooling load condition) and ending hours (cooling load rapid reduction condition) to achieve high running efficiency. Figs. 2a, 2b show the characteristics of the cooling load during the two scenarios.

Night hours (Fig. 2a): During 10 pm and 5 am, the cooling load is only half of the rated capacity of a chiller. Consequently, the chiller operates with low efficiency throughout the night. Ending hours (Fig. 2b): Between 6 pm and 8:30 pm, the cooling load is slightly over the rated capacity. Two chillers are needed in such conditions. This results in two operating chillers running at a lower PLR. A new control strategy is needed to enhance the chiller efficiency during this period.

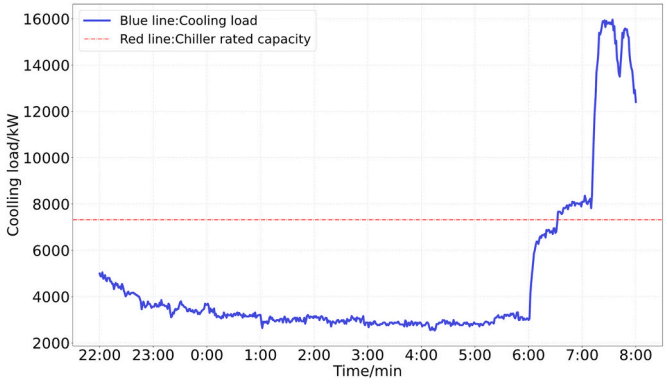

Fig. 2a. Cooling load of the studied high-rise commercial building during night hours.

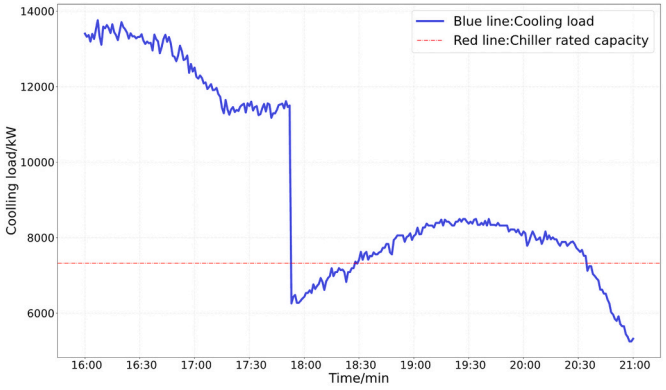

Fig. 2b. Cooling load of the studied high-rise commercial building during the ending hours.

2.2. *Basic logic of night hours control strategy – night hour mode*

The proposed night-hour mode consists of three steps: the initial step, the charging step, and the discharging step. In the initial step, the chiller number is determined based on the real-time building cooling demand. During the charging step, the supply chilled water temperature set-point is reduced so that the system's inherent cold storage can provide higher storage capacity. In the discharging step, all chillers are shut down, and the building is only cooled by the cooling energy stored in the chilled

water delivery system. Typically, the charging and discharging cycles are expected to occur 1–3 times per night, within acceptable operational limits.

Fig. 3 demonstrates the framework of the night hour mode. The control strategy will anticipate the discharging time if a singular chiller is active with a small value Z (typically below 70 %). This prediction aims to ensure the sustained thermal comfort of the building during periods when all chillers are deactivated, relying on stored cooling energy to meet the cooling demand. The prediction of the discharging time is based on the energy balance equation presented by Eq. (1).

$$3600 \bullet \int_0^{T_{off}} CL(t)d_t = C_{TES} \bullet \Delta T \quad (1)$$

where t_{off} ($hour$) is the hours to be predicted. $CL(t)$ (kW) is the building cooling load profile predicted previously. C_{TES} (kJ/K) is the thermal capacitance of the virtual thermal mass representing the thermal storage effect of the chilled water delivery system. ΔT (K) is the allowed temperature increase of the chilled water.

The prediction of t_{off} involves the estimation of the cooling load from the present time to 1 h into the future. A data-driven model (discussed in a subsequent section) is utilized to predict the cooling load in the short future. If the t_{off} exceeds 1 h, the charging step will be initiated. The supply chilled water temperature will be set to $T_{sup,low}$ (i.e., 5.5 °C in this case). Once the supply chilled water temperature reaches its set point, and the ΔT ($\Delta T = T_{rtn}$ - T_{sup}) is lower than ΔT_{min} (i.e., 3 K in this case), the discharging step is activated. The singular operational chiller, along with its corresponding primary and condensate pumps, will be deactivated. The secondary chilled water pumps will continue to maintain chilled water recirculation. It should be noted that the chilled water will flow through the bypass line in the reverse direction compared to normal mode. When the supply chilled water temperature remains higher than $T_{sup,high}$(i.e., 10 °C in this case) for 30 s, the normal mode will be activated. In this case, it is assumed that the stored cooling energy has been used up, and a chiller needs to be brought into operation to maintain building thermal comfort.

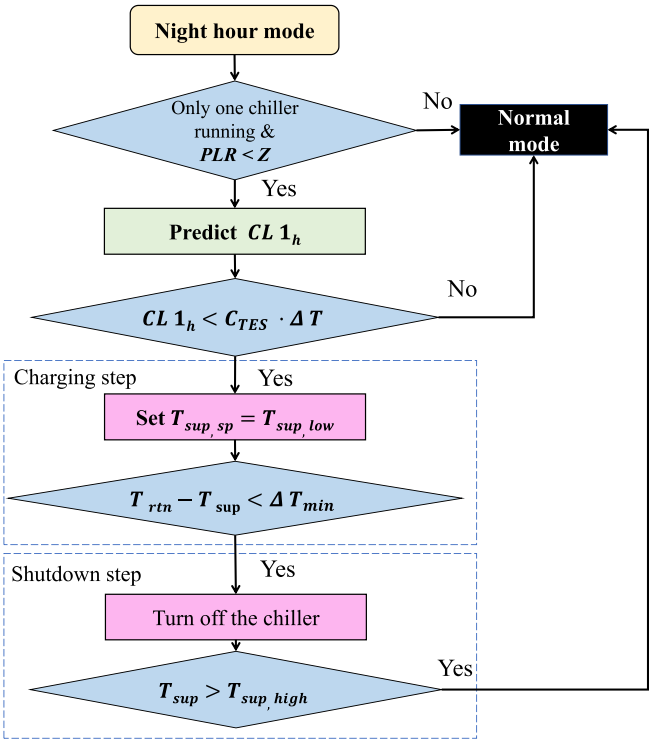

$CL_{real-time}$: Real time cooling load
CL_{1h}: Cooling load for the next hour
C_{TES}: Thermal capacitance of chilled water delivery system
Q_{CAP}: Chiller's cooling maximum capacity
ΔT_{min}: Minimum feasible temperature difference between chilled supply and return water.
T_{rtn}: Measured turn chilled water temperature
T_{sup}: Measured supply chilled water temperature
$T_{sup,sp}$: Supply chilled water temperature set-point
$T_{sup,low}$: Supply chilled water temperature minimum set-point
$T_{sup,high}$: Supply chilled water temperature maximum feasible point

Fig. 3. Framework of the proposed chiller night hour mode.

2.3. Basic logic of ending hours control strategy – ending hour mode

The ending-hour mode also consists of three distinct operational steps: the initial step, the charging step, and the discharging step, as shown in Fig. 4 This strategy enhances the operational efficiency of the chiller by optimizing its runtime and fine-tuning the temperature of the supplied chilled water. The working principles of the chiller in the initial and charging steps are similar to the night-hour mode. In the discharging step, the cooling is simultaneously supplied by the operating chillers and the system's inherent cold storage.

The ending hour mode is activated when the chiller's PLR drops to Z (typically below 70 %). It indicates a situation where the cooling load of the building requires multiple chillers to operate simultaneously, but each with a relatively low PLR. Typically, this situation would happen during the ending hours, when the cooling load of the building drops rapidly, and the charging step will be initiated. The supply chilled water temperature of all operation chillers will be set to $T_{sup,low}$ (i.e., 5.5 °C in this case). When the chilled water supply reaches its set-point, and the ΔT ($\Delta T = T_{rtn}$ - T_{sup}) is lower ΔT_{min} (i.e., 3 K in this case), the discharging step is activated. One of the operating chillers is shut down, and the supply chilled water temperature set-point is reset to $T_{sup,rated}$ (i.e., 7 °C in this case). If the cooling load is lower than the rated cooling capacity of one chiller, the system will enter night hour mode. If the supply chilled water temperature exceeds $T_{sup,high}$(i.e., 10 °C in this case), the system switches to normal mode (i.e., one chiller needs to be put into operation).

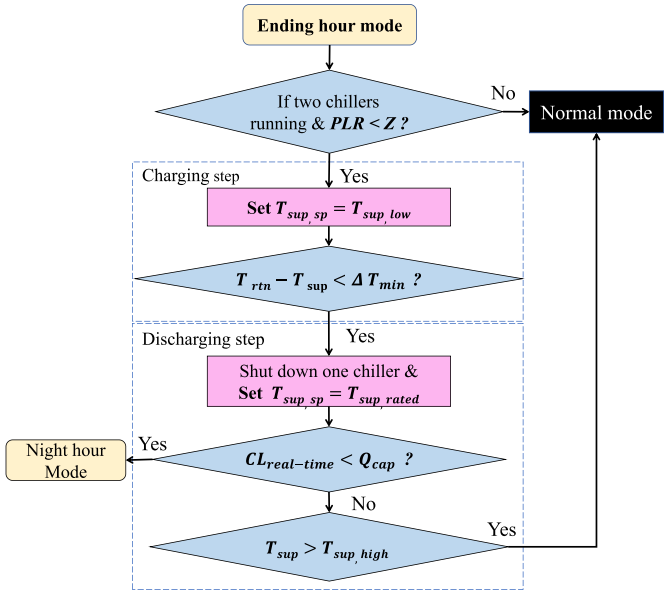

$CL_{real-time}$: Real time cooling load
C_{TES}: Thermal capacitance of chilled water delivery system
T_{rtn}: Measured return chilled water temperature
T_{sup}: Measured supply chilled water temperature
ΔT_{min}: Minimum feasible temperature difference between chilled supply and return water.
Q_{CAP}: Chiller's cooling maximum capacity
$T_{sup,sp}$: Supply chilled water temperature set-point
$T_{sup,low}$: Supply chilled water temperature minimum set-point
$T_{sup,rated}$: Supply chilled water temperature rated set-point

Fig. 4. Framework of the proposed chiller ending hour mode.

2.4. Proposed data-driven model for short-term building cooling load prediction

The long short-term memory (LSTM) network, a specialized type of recurrent neural network (RNN), is employed in the night hour mode to predict short-term cooling loads based on historical cooling data, ensuring that the discharging process duration is maintained as expected during night hours. LSTM is particularly suited for time series prediction tasks, such as energy consumption, due to its ability to capture temporal dependencies within the data. Unlike traditional RNNs, LSTM effectively mitigates the vanishing and exploding gradient issues, which are common in long sequence data, thus enabling the network to retain long-term dependencies and provide accurate forecasts. [23-26].

In energy prediction applications, LSTM has been demonstrated superior performance over other models in previous study, including BPNN, ARMA, and ARFIMA. Jian et al. [24] have shown that LSTM provides higher prediction accuracy for periodic energy consumption compared to BPNN, ARMA models. Lin et al. [30] demonstrated that the LSTM algorithm was feasible for predicting long-term energy consumption without weather data. Although comparisons with alternative forecasting models could provide further insights, this study focuses specifically on utilizing the LSTM model within the context of chiller plant operations. The prediction performance is assessed by the most common used established metrics, such as CV-RMSE and MAE, to evaluate predictive accuracy and the suitability of the model.

Fig. 5 shows the proposed LSTM prediction operation framework. The LSTM model takes the previous 24 h data as inputs and predicts the future one-hour cooling load by the rolling forecast method [31,32]. The method predicts the next step, adds the predicted value to the input sequence, and subsequently removes the oldest data. This iterative process is repeated to predict subsequent values. By employing this rolling approach, the model can predict the cooling load data for the next hour. In the case study on the simulation platform, the LSTM model used for short-term cooling load prediction consists of one LSTM layer with 400 units to capture temporal dependencies in the data. The input shape is defined by the number of features and time steps, with data structured to reflect 24 h of past observations. A dense layer with a single neuron is used for the output. The model is trained using the Mean Squared Error (MSE) loss function and the Adam optimizer, with 500 epochs and a batch size of 72.

3. Description of the case study and validation platforms

3.1. The real high-rise commercial building and air-conditioning system

The proposed strategy is specifically tested and validated in the air-conditioning system of a high-rise commercial building in Hong Kong from April to May 2022. During this period, temperatures in Hong Kong typically range from 20.8 to 28.4 °C, extreme highs reaching 35 °C, while the relative humidity averages around 83 %, making it one of the most humid times of the year. This case study serves as a representative example to evaluate the feasibility and effectiveness of the control strategy within the context of a high-rise commercial building. While the approach can be broadly applicable to a variety of building types and climatic conditions, this study focuses on its implementation in a high-rise building to showcase its potential benefits and chiller performance under typical operational challenges. The test building is 490 m and consists of 108 floors. The structure comprises three main sections: a ground-level car park covering 24,000 m^2, shopping arcades spanning 67,000 m^2 across the first five floors, and a 230,000 m^2 tower above, housing commercial offices and a hotel situated beyond the 100th floor. A complex chilled water distribution network is designed to distribute

Table 1
Specifications of the main equipment in the system.

Chillers	N	$M_{w,ev}$ (L/s)	$M_{w,cd}$ (L/s)	CAP (kW)	W (kW)
WCC-06-01 to 06	6	345.0	410.1	7230	1346

Cooling towers	N	M_w (L/s)	M_a (m^3/s)	Q_{rej} (kW)	W (kW)
CTA-06-01 to 06	6	250.0	157.2	5234	152
CTB-06-01 to 05	5	194.0	127.0	4061	120

Pumps	N	M_w (L/s)	$Head$ (m)	η (%)	W (kW)
CDWP-06-01 to 06	6	410.1	41.60	83.6	202
PCHWP-06-01 to 06	6	345.0	31.60	84.5	126
SCHWP-06-01 to 02	1(1)[a]	345.0	24.60	82.2	101
SCHWP-06-03 to 05	2(1)[a]	345.0	41.40	85.7	163
SCHWP-06-06 to 08	2(1)[a]	345.0	30.30	84.2	122
SCHWP-42-01 to 03	2(1)[a]	294.0	36.50	87.8	120
SCHWP-42-04 to 06	2(1)[a]	227.0	26.20	84.3	69.1
SCHWP-78-01 to 03	2(1)[a]	227.0	39.20	85.8	102

[a] Values in round brackets indicate the number of standby pumps.

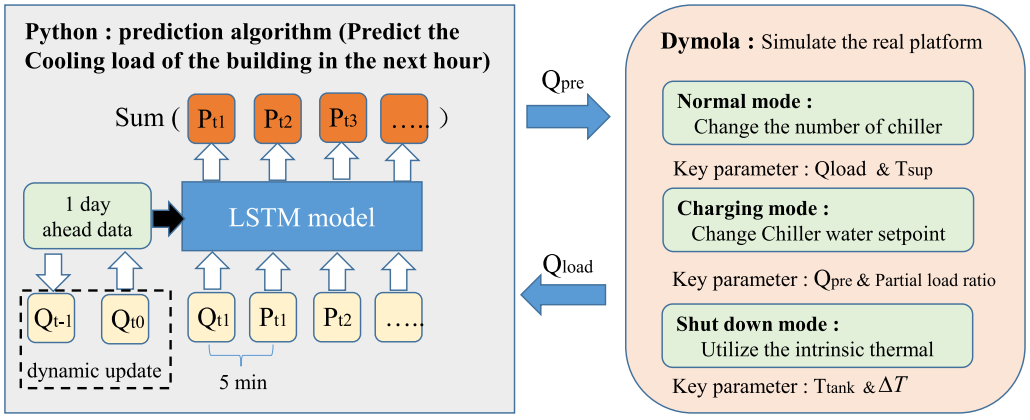

Q_{load} : real time cooling load from building T_{sup} : The temperature of chiller supply water

Q_{pre}: Cooling load forecast for the next hour

Fig. 5. The proposed LSTM prediction operation framework.

cooling energy from the chiller plant to all floors. The air-conditioning system serves all floors except the hotel above the 100th floor. Table 1 shows the detailed specifications of the main equipment.

The system consists of six identical high voltage (11,000 V) CSD chillers. Each chiller is associated with a primary chilled water pump and a cooling water pump, and both pumps are at constant speed. Eleven cooling towers provide chillers with cooling water. Each office floor consists of two AHUs, and the chilled water is delivered to each AHU via two sets of reverse return risers. Plate heat exchangers are used to isolate chilled water for individual zones to avoid high pressure in water pipes from gravity.

Table 2 provides a summary of the length and diameters of pipes in the real system. The total volume of water and pipe steel are estimated to be around 738 m^3 and 58 m^3, respectively. The total thermal capacitances of the water and pipe steel are 3,100,000 kJ/K and 212,600 kJ/K, respectively. As a result, the thermal capacitance of the system's inherent cold storage is estimated to be around 3,312,600 kJ/K. The actual capacitance of the system may be higher because the thermal capacitance of those AHU branches is not counted.

3.2. The dynamic simulation platform

A detailed dynamic platform is developed using Modelica based on the studied building air-conditioning system. The model constructed can be exported as a Functional Mock-up Unit (FMU) file, which can be recognized by other software, thereby enhancing reusability and interoperability between external models provided via Functional Mock-up Interface (FMI) and the Modelica environment [27]. Moreover, this work employs the package "pyfmi" for Python to establish a connection between the prediction algorithm and the simulation platform [28].

Fig. 6a shows the simulation platform built based on the Modelica Buildings library, including the physical system module and control strategy module [29]. The simulation module for the physical system encompasses several key components, including the multiple-chillers module, multiple-pumps module, cooling tower module, weather module, cooling load module, and a simplified thermal storage module. The Partial-Mixing-Volume module in the library is adopted to simulate the inherent cold storage. The proposed control strategy is programmed into a control strategy module, as shown in the Fig. 6b. The control strategy simulation module comprises the control mode selection, chiller number control, chilled water temperature set-point reset, and pump speed control. It is imperative to highlight that the control mode selection module takes the LSTM (deployed in Python) predicted cooling load as input. The predicted cooling load data seamlessly integrates into the control module at each simulation step, augmenting the system's overall efficacy.

Table 2
The length and diameters of the chilled water delivery system.

Pipelines	Length (m)	Number of pipes	Total length (m)	Diameter (mm)
Risers: M1 to Zone 1 floors	63.03	6	378.18	500
Risers: M1 to Zone 2 floors	127.47	6	764.82	500
Risers: M2 to Zone 3 floors	120.42	6	722.52	500
Risers: M3 to Zone 4 floors	106.89	6	641.34	400
Risers: M1 to M2	139.65	2	279.3	800
Risers: M2 to M3	120.42	2	240.84	600
Main pipes inside M1	60	2	120	800
Branch pipes to AHUs	10	2	1280	150

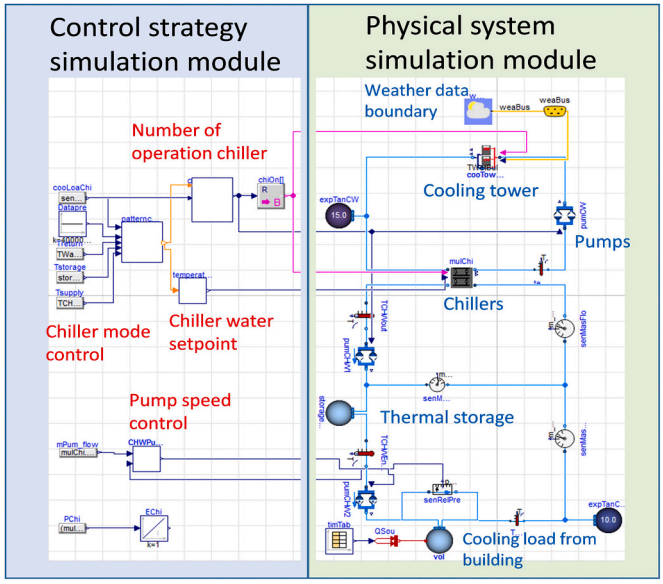

Fig. 6a. Implementation of the proposed control strategy in the simulation platform.

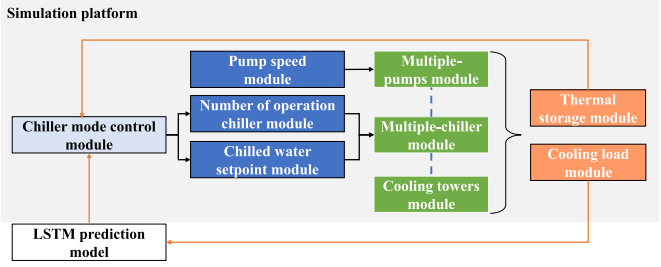

Fig. 6b. Flowchart of the modules in the simulation platform.

4. Test results and analysis

Section 4.1 presents the on-site proof of concept test results. Section 4.2 presents the validation results of the proposed night hour mode control. Section 4.3 presents the validation results of ending hour mode control.

4.1. On-site proof of concept (POC)

4.1.1. Night hour mode

The test was conducted in a high-rise commercial building on the night of 14/April/2022, a typical working day. As shown in Fig. 7, the supply chilled water temperature set-point was 5.5 °C at 23:00. It took 26 min to reach the set-point (at 11:26 pm). The only operating chiller was turned off at 00:33 am, and no chiller was in operation until 3:11 am when a chiller was put back into operation, and the supply chilled water temperature was reset to 8 °C. The total discharging time was 2 h and 38 min. As can be seen in Fig. 7, the temperatures T_{95}, T_{33}, and T_{16} increased by approximately 2 K during the first 10 min of the discharging period (As shown in Fig. 8, T_{95}, T_{33}, and T_{16} represent the supply chilled water temperature for Zone 2, Zone 3, and Zone 4, respectively). The increasing rate slowed down later, and the temperatures gradually reached around 11 °C. In normal operation, $T_{95} < T_{33} < T_{66}$. However, the lower zone water temperature could be higher than the upper zone during discharging.

An energy-saving analysis was performed by comparing the data between 10 pm and 6 am on the test day with a reference day (15/April/2022) when the building load profiles were similar. Fig. 8(a) and (b)

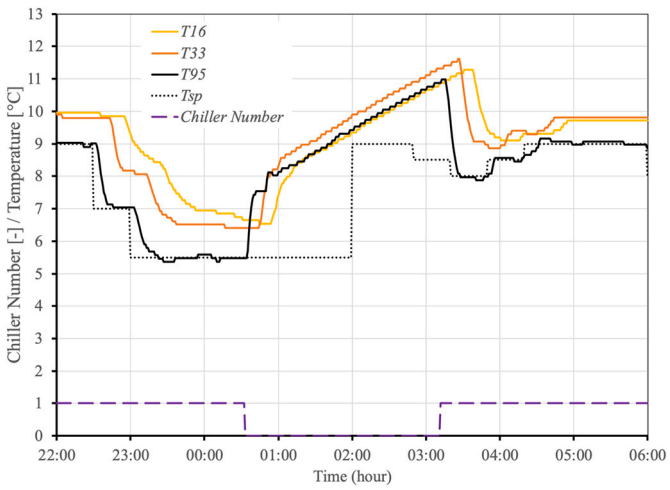

Fig. 7. Supply chilled water temperature to different zones (T_{16}, T_{33}, T_{95}), chiller supply chilled water temperature set-point (T_{sp}), and operating chiller.

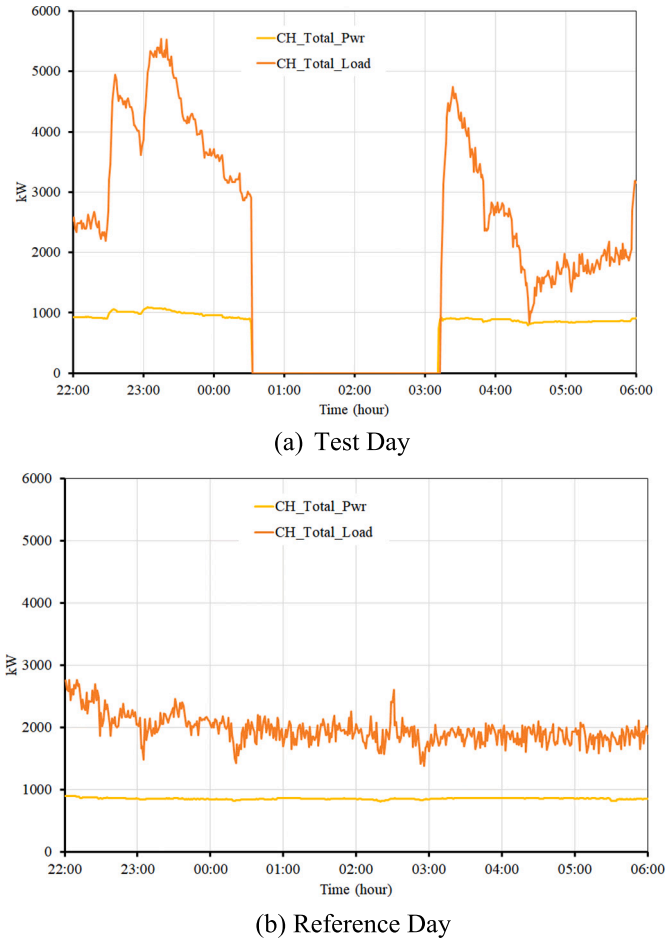

Fig. 8. Comparison of measured chiller load and chiller power during the test day and the reference day.

present the measured chiller load and chiller power during the test day and the reference day, respectively.

As shown in Fig. 8(a), the building cooling load was shifted from the discharging period to the neighbouring periods on the test day. Despite the loading increase before and after the discharging period, there was no obvious change in chiller power consumption. By contrast, the chiller load and power consumption varied slightly around constant values on the reference day. The chiller load was around 2000 kW, and power consumption was around 850 kW. Table 3 presents the summarized data on chiller efficiency for the two days. In comparison with the Reference Day, despite a 2.9 % increase in total cooling load during the test, the total chiller power consumption decreased significantly by 28.1 %, and the total chiller COP improved by 43.3 %.

The total chiller power consumption was reduced by 1931 kWh. During the discharging period, the cooling towers, primary chilled water pumps, and condenser water pumps were also turned off. The savings in primary chilled water pumps and condenser water pumps were 206 kWh and 330 kWh, respectively, and the cooling tower fan energy was reduced by 41 kWh. The total energy saving was around 2508 kWh during the tested night.

4.1.2. Ending hour mode

The ending-hour mode was tested on a normal working day (20 May 2022). Fig. 9 shows the chiller supply chilled water temperature set-point, the supply chilled water temperature for different zones, and the operating chiller number. At 16:30, when two chillers were in operation, the chiller supply chilled water temperature was reset from 7 °C to 5.5 °C. About 1 h later, one of the two running chillers was turned off.

During the on-site test, when one chiller was turned off, the cooling load was higher than the maximum capacity of the remaining operating chillers. The only chiller was operating at its maximum capacity, and the supply of chilled water temperature began to increase. There was a brief drop in T_{95} due to a reduction in cooling load when some of the AHUs automatically closed at 18:00. However, the cooling load in the upper zones did not decrease significantly, and T95 quickly returned to its original level due to heat transfer via plate heat exchangers. The increasing trend in the supply of chilled water temperature continued until 19:00 when most office workers left. Despite the slightly high supply of chilled water temperature during the test, no complaints about thermal comfort were received, indicating that the building's thermal comfort was not compromised.

The total chiller loading is shown in Fig. 10. The charging process began at 16:30 and ended at 17:28. Both chillers were running at their maximum capacity during this period. Notably, the total chiller power increased slightly after the reset of the chiller supply chilled water temperature set-point. It dropped dramatically after the shutdown of a chiller at 17:28.

Fig. 11 shows the total chiller COP during the on-site test. The total COP increased slightly due to higher PLR after 16:30 when the chiller supply chilled water temperature is reset lower. It further increased from around 6.0 to around 6.5 when one chiller was turned off at 17:28.

The energy-saving analysis focused on the period between 16:00 and 19:00 when the charging and discharging processes occurred. The total chiller load and electricity consumption during these 3 h were 35,979 kWh and 5844 kWh, respectively, with an average chiller COP of 6.15. To assess the energy savings attained through the implemented control strategy, a day with a similar cooling load was chosen as the reference Day. The mean cooling load between 16:00 and 19:00 was 11,993 kWh during this reference day. The average chiller COP on the reference day was 5.7. As shown in Table 4, the chiller power consumption was reduced by 468 kWh. The savings in primary chilled water pumps, condenser water pumps, and cooling towers were 189 kWh, 303 kWh,

Table 3
Comparison of chiller efficiency.

	Total load (kWh)	Total chiller power (kWh)	Total chiller COP
Test day	16,226	4929	3.292
Reference day	15,765	6860	2.298
Difference	461 / 2.9 %	−1931 / -28.1 %	0.994 / 43.3 %

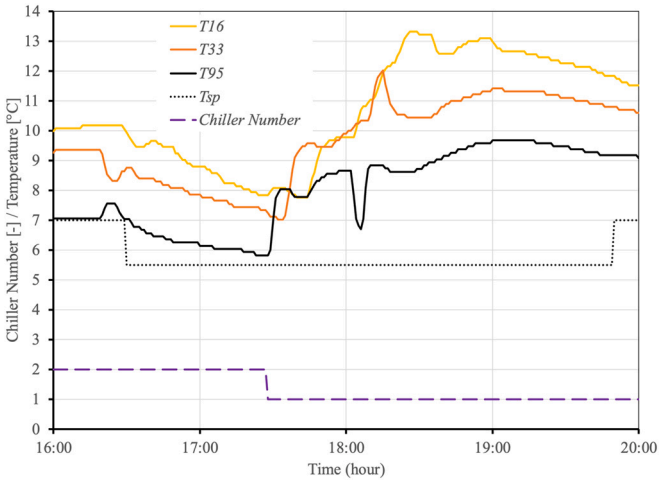

Fig. 9. Supply chilled water temperature to different zones, chiller supply chilled water temperature set-point, and operating chiller number.

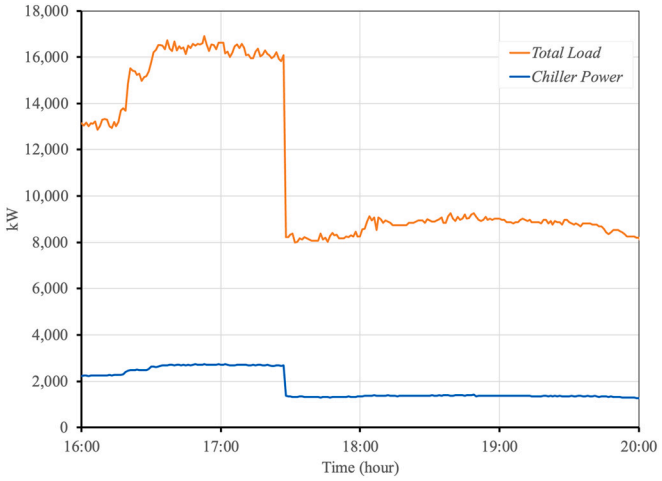

Fig. 10. Total chiller load and total chiller power on the test day.

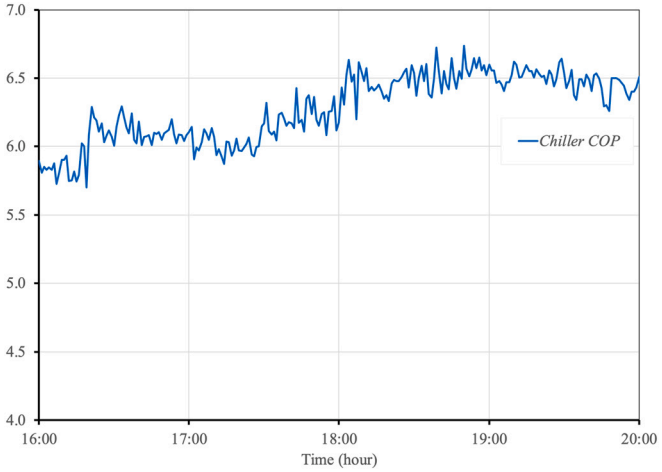

Fig. 11. Total chiller COP on the test day.

Table 4
Energy savings from equipment.

	Chiller	Pump	Cooling tower	Total
Energy saving (kWh)	468	189	303	998

and 38 kWh, respectively. The total saving was calculated to be 998 kWh, accounting for an overall saving rate of 14 %.

4.2. Simulation validation results

4.2.1. Accuracy of the LSTM for short-term cooling load prediction

In night-hour mode, the LSTM model is utilized to estimate the total cooling demand for the following hour. To assess the model's precision, comparisons are made between the predicted cooling load and the actual cooling load measurements obtained afterwards. Fig. 12 illustrates the comparative analysis between the observed and predicted cooling loads of the building during night hours. It is evident from Fig. 11 that the LSTM model achieves relatively accurate predictions when it incorporates the cooling load data of just one day ahead as its input variables.

To evaluate the feasibility of this prediction model, two statistical metrics are employed: the Mean Absolute Error (MAE) and the Coefficient of Variation of the Root Mean Square Error (CV-RMSE), as shown in Eqs. (2) and (3), respectively. The MAE calculates accuracy by averaging the error between predicted and actual values. Expressed as a percentage, the CV-RMSE assesses model accuracy by considering the deviation between predicted and actual values relative to the data size. Predictive models with deviations below 15 % are deemed viable [30].

$$\mathrm{MAE} = \frac{1}{n}\sum_{k=1}^{n}\left|y(k) - y_p(k)\right| \tag{2}$$

$$\mathrm{CV-RMSE} = \frac{1}{\bar{y}}\sqrt{\frac{\sum_{k=1}^{n}\left(y(k) - y_p(k)\right)^2}{n}} \tag{3}$$

where $y(k)$ and $y_p(k)$ are the actual and the predicted values respectively, and $\bar{y}$ denotes the average values. The accuracy results of the model are as follows, with an MAE value of 338.2 kWh; and a CV-RMSE value of 12.6 %, which testify to the accuracy of the prediction model.

4.2.2. Simulation validation result of the night hour mode

As aforementioned, night-hour mode is applied for high cooling capacity chillers operating under low PLR conditions at night. Under the conventional control strategy, one chiller run continuously at night to cool the building. The supply chilled water temperature stabilized at around 7.2 °C. Under night-hour mode, the supply chilled water

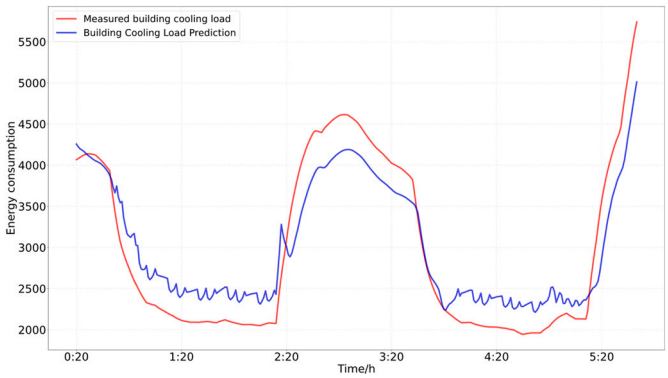

Fig. 12. Predicted result of the high-rise commercial building cooling loads at night.

temperature fluctuates within the range of 6–10 °C from 11:00 pm to 7:00 am. These temperature fluctuations are indicative of storage cycles, with chiller plant systems typically experiencing two to three such cycles per night.

Fig. 13 shows the results of the chiller's COPs in the night hour mode and conventional mode. The red and green curves represent the chiller COP under conventional mode and the night hour mode, respectively. Between 10:00 pm and 5:00 am the next day, the chiller's COP under conventional mode was around 3.0, significantly lower than its rated value of 5.68. By contrast, in night-hour mode, the chiller's COP varies between 4.7 and 5.9 when the chiller was in operation.

Table 5 presents the cooling system's energy consumption from 9 pm to 7 am the following day. Compared with the conventional strategy, the night-hour mode achieved significant savings of 4747.6 kWh from the chiller plant. Energy savings for the primary chilled water pumps and condenser water pumps were also achieved due to reduced operation time. In summary, the utilization of the proposed night-hour mode achieved an overall energy saving of approximately 4785 kWh and 5728.1 HK$ over the 10-h night period, resulting in a significant energy consumption reduction of 34.69 %.

4.2.3. 4.2.3 Simulation validation result of the ending hour mode

As mentioned previously, the cooling demand declines swiftly during the ending hours. When the conventional strategy is applied, the chiller COP decreases with the reduction of cooling demand. The supply chilled water temperature is maintained at a constant value with the conventional control. On the other hand, the commencement of the charging process in the proposed ending-hour mode occurs around 5:30 pm, leading to a decline in the supply chilled water temperature. At approximately 7:20 pm, all chillers are deactivated, and the discharging process is activated, leading to a gradual increase in the supply chilled water temperature.

Fig. 14 compares the chillers' COP and chiller number under the proposed ending-hour mode and conventional mode. Under the conventional mode, depicted by the red curve, the chillers operate persistently with a lower COP. By contrast, when the ending-hour mode is applied, the system switches to the charging process when the cooling load is decreases rapidly. During this step, the chiller operates at a high PLR, significantly increasing the chiller COP. Approximately 20 min later, when the system's inherent cold storage is fully charged, one of the operating chillers is shut down. The remaining chiller operates with an even higher COP due to the higher loading. No chiller consumes energy when the discharging process is activated after 19:20. Table 6 shows the energy savings of the proposed control strategy. The savings in chillers and pumps are 66.26 kWh and 41.12 kWh, respectively. The total savings are 107.38 kWh, leading to an energy-saving percentage of approximately 27.09 %, and in Hong Kong 128.5 HK$ can be saved during every ending hour. It can be affirmed that the ending-hour mode is an effective strategy for reducing energy consumption during the ending hours.

Table 5
Power Consumption from the equipment of different strategies.

Power consumption (kWh)	Chiller consumption	Pump consumption	Total consumption
Night hour mode	8953.7	54.4	9008.1
Conventional mode	13,701.2	91.88	13,793.1
Savings	4747.6	37.48	4785.0 (34.69 %)

4.3. Discussion of the on-site POC tests and simulation validation tests

Fig. 15 presents a comparison of the COP results from on-site POC tests and simulation validation tests. The chiller COP has been improved during both night hours and ending hours. Compared to previous strategies utilizing VSD chillers and larger TES systems, which achieved energy savings between 3.10 % and 22.94 % [8], and another study where the proposed control strategy resulted in 2.10 % to 5.15 % energy

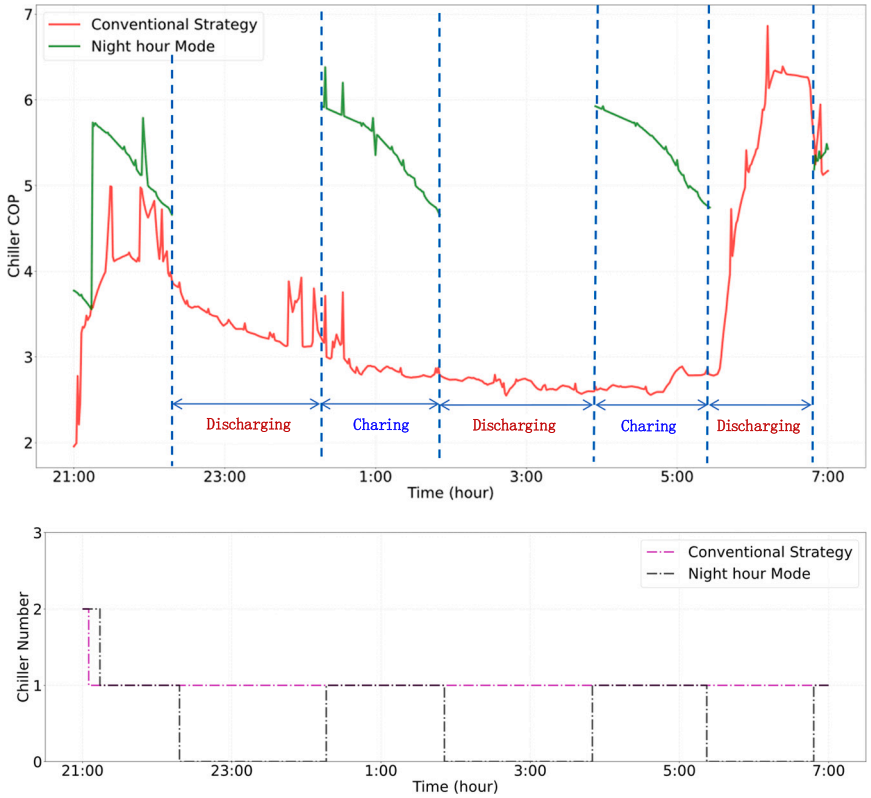

Fig. 13. Different chiller COPs and chiller numbers under different strategies.

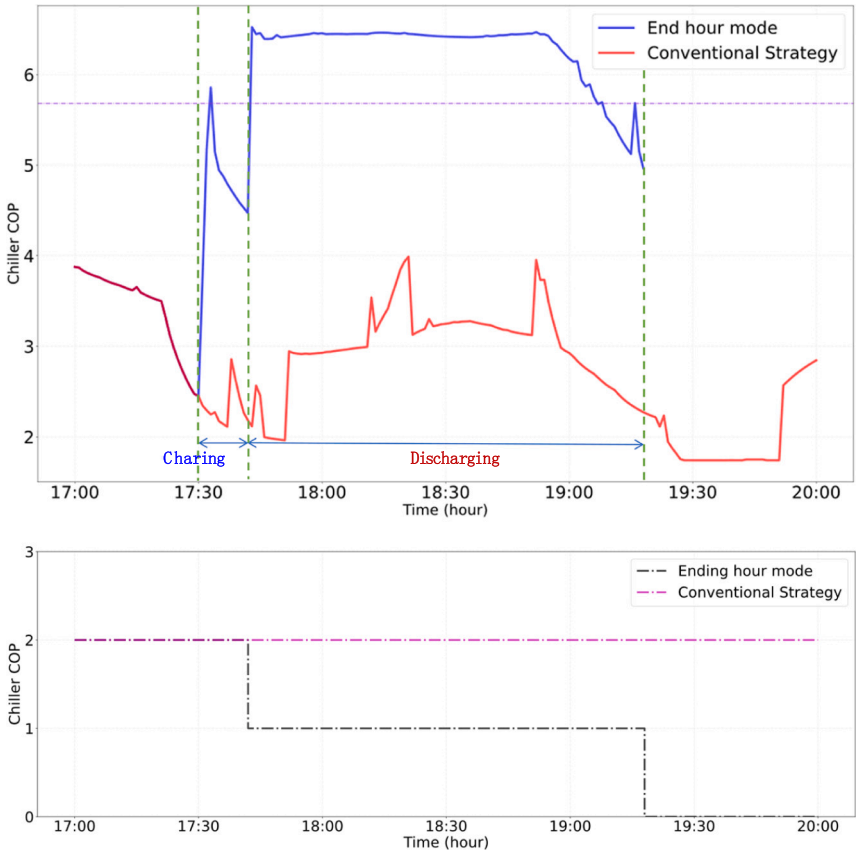

Fig. 14. Comparison of the chiller COPs and chiller numbers for different strategies during the ending hours.

Table 6
Power Consumption of the main equipment during 17:00–20:00 in the test.

Power consumption (kWh)	Chiller consumption	Pump consumption	Total consumption
Ending hour mode	222.68	66.26	288.94
Conventional mode	288.94	107.38	396.32
Savings	66.26	41.12	107.38 (27.09 %)

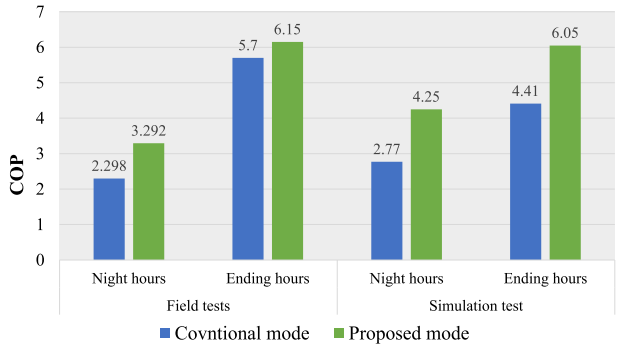

Fig. 15. Comparison of the chiller COP result on the field test and simulation test.

savings [15], the chiller plant efficiency improved significantly under the proposed control mode during both night hours and the ending hours. The proposed control strategy enhanced chiller efficiency by 30.7 % during night hours and 22.9 % during ending hours on the simulation tests, while achieve 28 % and 14 % energy saving on the field tests.

These differences between on-site tests and simulation tests can be ascribed to three primary factors. First, the weather conditions and test durations are different; the field tests were conducted between April and May, while the simulation utilized cooling load data from the test building in August. Secondly, the complete control strategy is tested in the simulation platform, while the on-site test only provides the concept validation. Thirdly, the simulation platform is constructed based on models with some simplifications. Though the accuracy is acceptable, the models still could not fully represent the real system. It is crucial to acknowledge that such differences are common and do not undermine the efficacy of the applied strategies. Despite these variations, the on-site POC test and simulation test results confirmed the effectiveness and potential advantages of the implemented strategy.

5. Conclusion

This paper presents two innovative control strategies, namely night-hour mode and ending-hour mode, aiming to enhance the energy efficiency of chiller plants under low PLR. These strategies leverage the inherent cold storage capabilities of the chilled water distribution systems in high-rise commercial buildings. The night-hour mode is designed to address the chiller inefficiencies during night hours, while the ending-hour mode is tailored to tackle the inefficiencies during ending hours.

The results of the on-site POC tests on the large and complex HVAC system in a high-rise commercial building show that the night-hour mode can improve the chiller COP by 43.3 % during the summer night hours. Meanwhile, the ending-hour mode can reduce the chiller energy consumption by 8 % and increase the overall efficiency of the chiller plant by 14 % during summer ending hours. These on-site POC test results confirm that the inherent cold storage of the system can be

utilized to enhance the efficiency of chiller plants. Simulation test results revealed that the night-hour mode with the predictive model (LSTM) can increase chiller efficiency by 30.7 %, corresponding to 4747.55 kWh of energy saving during a summer night. The proposed ending-hour mode increases chiller efficiency by 22.9 % at the ending hours, corresponding to 66.26 kWh of energy saving.

It is also worth noting that the proposed control strategies are simple and effective and do not require additional equipment costs. They are particularly applicable for large and complex HVAC systems with an extensive chilled water distribution network with high thermal capacity. The strategies are also suitable for a chiller plant with oversized chillers where the chiller plant has to run at low PLR in some low-load conditions.

However, it is also necessary to point out the limitations in implementing the proposed control strategies. In the case of night-hour mode, a single chiller underwent a few separate start-stop cycles throughout the night. While the proposed strategy is expected to enhance the system efficiency, the start-stop cycles of the chiller may be a concern for long-term reliability. If the cycle number is too high, it may cause the chiller to degrade. The acceptable chiller start-stop intervals need to be carefully determined before the practical implementation of the proposed control strategies. Additionally, future research could incorporate a comprehensive financial analysis to evaluate the operational and investment costs associated with these strategies, providing a clearer understanding of potential cost savings and return on investment.

CRediT authorship contribution statement

Xiaoyu Lin: Visualization, Validation, Software, Formal analysis, Writing – original draft. **Kui Shan:** Supervision, Resources, Methodology, Investigation, Data curation, Conceptualization, Writing – review & editing. **Shengwei Wang:** Supervision, Project administration, Methodology, Funding acquisition, Conceptualization, Writing – review & editing.

Declaration of competing interest

The authors declare that they have no known competing financial interests or personal relationships that could influence the work reported in this paper.

Acknowledgement

The work described in this paper is fully supported by a grant from the Research Grants Council of the Hong Kong Special Administrative Region, China (Project No. PolyU 15205321). The authors also would like to thank the support of Kai Shing Management Services Limited for on-site tests and data collection.

Data availability

The authors do not have permission to share data.

References

[1] K. Shan, S. Wang, D. Gao, F. Xiao, Development and validation of an effective and robust chiller sequence control strategy using data-driven models, Autom. Constr. 65 (2016) 78–85, https://doi.org/10.1016/j.autcon.2016.01.005.

[2] R. Jing, M. Wang, R. Zhang, N. Li, Y. Zhao, A study on energy performance of 30 commercial office buildings in Hong Kong, Energ. Buildings 144 (2017) 117–128, https://doi.org/10.1016/j.enbuild.2017.03.042.

[3] S. Birkha Mohd Ali, M. Hasanuzzaman, N.A. Rahim, M.A.A. Mamun, U. H. Obaidellah, Analysis of energy consumption and potential energy savings of an institutional building in Malaysia, Alex. Eng. J. 60 (1) (2021) 805–820, https://doi.org/10.1016/j.aej.2020.10.010.

[4] J. Deng, W. Qiang, C. Peng, Q. Wei, H. Zhang, Research on systematic analysis and optimization method for chillers based on model predictive control: a case study, Energ. Buildings 285 (2023) 112916, https://doi.org/10.1016/j.enbuild.2023.112916.

[5] I.N. Suamir, I.N. Ardita, I.M. Rasta, Effects of cooling tower performance to water cooled chiller energy use: A case study toward energy conservation of office building, in: In *2018 International Conference on Applied Science and Technology (iCAST)*, IEEE, Manado, Indonesia, Oct. 2018, pp. 712–717, https://doi.org/10.1109/iCAST1.2018.8751530.

[6] W.T. Ho, F.W. Yu, Determinants of low energy performance in a multi-chiller system serving an educational premise, Int. J. Refrig. 114 (2020) 47–53, https://doi.org/10.1016/j.ijrefrig.2020.02.019.

[7] M. Saleh Kandezi, S.M. Mousavi Naeenian, Investigation of an efficient and green system based on liquid air energy storage (LAES) for district cooling and peak shaving: energy and exergy analyses, Sustain Energy Technol Assess 47 (2021) 101396, https://doi.org/10.1016/j.seta.2021.101396.

[8] K. Shan, C. Fan, J. Wang, Model predictive control for thermal energy storage assisted large central cooling systems, Energy 179 (2019) 916–927, https://doi.org/10.1016/j.energy.2019.04.178.

[9] K. Roth, J. Brodrick, Cool thermal energy storage[J], ASHRAE J. 48 (9) (2006) 94–96.

[10] E. Oró, M. Codina, J. Salom, Energy model optimization for thermal energy storage system integration in data centres, J. Energy Storage 8 (2016) 129–141, https://doi.org/10.1016/j.est.2016.10.006.

[11] B. Turgut, D. Erdemir, N. Altuntop, An experimental investigation of the effects of the number of capsules and operating conditions on the performance of encapsulated ice storage system, J. Energy Storage 64 (2023) 107206, https://doi.org/10.1016/j.est.2023.107206.

[12] V. Ghamari, H. Hajabdollahi, M. Shafiey Dehaj, A. Saleh, Investigating the effect of energy storage tanks on thermoeconomic optimization of integrated combined cooling, heating and power generation with desalination plant, J. Energy Storage 56 (2022) 106120, https://doi.org/10.1016/j.est.2022.106120.

[13] E. Bellos, et al., Dynamic investigation of centralized and decentralized storage systems for a district heating network, J. Energy Storage 56 (2022) 106072, https://doi.org/10.1016/j.est.2022.106072.

[14] A. Anderson, B. Rezaie, M.A. Rosen, An innovative approach to enhance sustainability of a district cooling system by adjusting cold thermal storage and chiller operation, Energy 214 (2021) 118949, https://doi.org/10.1016/j.energy.2020.118949.

[15] W. Zou, Y. Sun, D. Gao, X. Zhang, Globally optimal control of hybrid chilled water plants integrated with small-scale thermal energy storage for energy-efficient operation, Energy 262 (2023) 125469, https://doi.org/10.1016/j.energy.2022.125469.

[16] Z. Ma, S. Wang, Supervisory and optimal control of central chiller plants using simplified adaptive models and genetic algorithm, Appl. Energy 88 (1) (2011) 198–211, https://doi.org/10.1016/j.apenergy.2010.07.036.

[17] S. Wang, D. Gao, Y. Sun, F. Xiao, An online adaptive optimal control strategy for complex building chilled water systems involving intermediate heat exchangers, Appl. Therm. Eng. 50 (1) (2013) 614–628, https://doi.org/10.1016/j.applthermaleng.2012.06.010.

[18] Y. Chen, C. Yang, X. Pan, D. Yan, Design and operation optimization of multi-chiller plants based on energy performance simulation, Energ. Buildings 222 (2020) 110100, https://doi.org/10.1016/j.enbuild.2020.110100.

[19] P. Huang, G. Augenbroe, G. Huang, Y. Sun, Investigation of maximum cooling loss in a piping network using Bayesian Markov chain Monte Carlo method, J. Build. Perform. Simul. 12 (2) (2019) 117–132, https://doi.org/10.1080/19401493.2018.1487998.

[20] C. Yan, S. Wang, C. Fan, F. Xiao, Retrofitting building fire service water tanks as chilled water storage for power demand limiting, Build. Serv. Eng. Res. Technol. 38 (1) (2017) 47–63, https://doi.org/10.1177/0143624416669553.

[21] M. Dai, H. Li, S. Wang, Event-driven demand response control of air-conditioning to enable grid-responsive buildings, Autom. Constr. 150 (2023) 104815, https://doi.org/10.1016/j.autcon.2023.104815.

[22] B.M. Seo, K.H. Lee, Detailed analysis on part load ratio characteristics and cooling energy saving of chiller staging in an office building, Energ. Buildings 119 (2016) 309–322, https://doi.org/10.1016/j.enbuild.2016.03.067.

[23] Y. Ding, Q. Zhang, T. Yuan, F. Yang, Effect of input variables on cooling load prediction accuracy of an office building, Appl. Therm. Eng. 128 (2018) 225–234, https://doi.org/10.1016/j.applthermaleng.2017.09.007.

[24] J.Q. Wang, Y. Du, J. Wang, LSTM based long-term energy consumption prediction with periodicity, Energy 197 (2020) 117197, https://doi.org/10.1016/j.energy.2020.117197.

[25] B. Mu, C. Peng, S. Yuan, L. Chen, ENSO forecasting over multiple time horizons using ConvLSTM network and rolling mechanism, in: In *2019 International Joint Conference on Neural Networks (IJCNN)*, IEEE, Budapest, Hungary, Jul. 2019, pp. 1–8, https://doi.org/10.1109/IJCNN.2019.8851967.

[26] Y. Liu, H. Wang, W. Feng, H. Huang, Short term real-time rolling forecast of Urban River water levels based on LSTM: a case study in Fuzhou City, China, Int. J. Environ. Res. Public Health 18 (17) (2021) 9287, https://doi.org/10.3390/ijerph18179287.

[27] T. Schmitt, M. Andres, S. Ziegler, and S. Diehl, "A Novel Proposal on how to Parameterize Models in Dymola Utilizing External Files under Consideration of a Subsequent Model Export using the Functional Mock-Up Interface," presented at the The 11th International Modelica Conference, Sep. 2015, pp. 23–29. doi:https://doi.org/10.3384/ecp1511823.

[28] S. Wilfling, B. Falay, Q. Alfalouji, and G. Schweiger, "A Dymola-Python framework for data-driven model creation and co-simulation," Presented at the Asian Modelica Conference 2022, Tokyo, Japan, November 24–25, 2022, Nov. 2022, pp. 165–170. doi:https://doi.org/10.3384/ecp193165.

[29] M. Wetter, M. Bonvini, T. S. Nouidui, W. Tian, and W. Zuo, "MODELICA BUILDINGS LIBRARY 2.0", doi: 10.26868/25222708.2015.2405.
[30] F. Dong, J. Yu, W. Quan, Y. Xiang, X. Li, F. Sun, Short-term building cooling load prediction model based on DwdAdam-ILSTM algorithm: a case study of a commercial building, Energ. Buildings 272 (2022) 112337, https://doi.org/10.1016/j.enbuild.2022.112337.
[31] B. Mu, C. Peng, S. Yuan, L. Chen, ENSO Forecasting over Multiple Time Horizons Using ConvLSTM Network and Rolling Mechanism, in: International Joint Conference on Neural Networks (IJCNN), IEEE, Budapest, Hungary, 2019, pp. 1–8, https://doi.org/10.1109/IJCNN.2019.8851967.
[32] Y. Liu, H. Wang, W. Feng, H. Huang, Short Term Real-Time Rolling Forecast of Urban River Water Levels Based on LSTM: A Case Study in Fuzhou City, China, Int. J. Environ. Res. Public. Health 18 (17) (2021) 9287, https://doi.org/10.3390/ijerph18179287.